



Multi-field merit-function-based regression method for Wide Field Infrared Survey Telescope grism system alignment

MARGARET Z. DOMINGUEZ,^{1,2,7} HYUKMO KANG,² SEONGHUI KIM,³ JOSHUA BERRIER,⁴ VICTOR J. CHAMBERS,¹ QIAN GONG,¹ JOHN G. HAGOPIAN,⁴ CATHERINE T. MARX,¹ LAURIE SEIDE,⁵ AND DAE WOOK KIM^{2,6,*}

¹NASA Goddard Space Flight Center, 8800 Greenbelt Rd, Greenbelt, Maryland 20771, USA

²James C. Wyant College of Optical Sciences, University of Arizona, 1630 E. University Blvd., Tucson, Arizona 85721, USA

³Korea Aerospace Research Institute, 169-84 Gwahak-ro, Yuseong-gu, Daejeon 34133, South Korea

⁴Tech Innovations LLC, PO Box 151, Glenwood, Maryland 21738, USA

⁵SGT Inc., 7701 Greenbelt Rd, Suite 400, Greenbelt, Maryland 20770, USA

⁶Department of Astronomy and Steward Observatory, University of Arizona, 933 N. Cherry Ave., Tucson, Arizona 85719, USA

⁷e-mail: margaret.z.dominguez@nasa.gov

*Corresponding author: letter2dwk@hotmail.com

Received 18 April 2019; revised 25 June 2019; accepted 29 July 2019; posted 30 July 2019 (Doc. ID 365492); published 26 August 2019

The grating prism (grism), slitless spectrometer aboard the Wide Field Infrared Survey Telescope enables a survey of emission-line galaxies. To facilitate its opto-mechanical alignment, a six-degree-of-freedom element was fabricated using alignment fiducials and integral flats and used to measure a wavefront by using an infrared interferometer placed at various field points over a 20×14 deg field of view in the grism coordinate frame. Modeling identified E2 to be the most sensitive element to the grism wavefront error and was used to efficiently align the system. The merit function regression method for a wide field of view was further used to verify the higher efficiency and accuracy of the proposed alignment technique compared with the conventional sensitivity table method. © 2019 Optical Society of America

<https://doi.org/10.1364/AO.58.006802>

1. INTRODUCTION

The precision alignment of optical systems with relatively small fields of view (FOVs) has historically been achieved by on-axis interferometry [1,2]. However, the process is lengthy and time-consuming for the alignment of optical systems with relatively large FOVs. For example, when aligning the Wide Field Infrared Survey Telescope (WFIRST) grating prism (grism) [3], which is a four-element refractive optics system, the wavefront errors (WFEs) observed at the extreme edges can be large, although the root mean square (RMS) of the WFEs of the on-axis measurement may be low. This is because of the presence of coma-zero conditions in non-symmetrical optical systems, resulting in misalignment possibly not noticeable in on-axis measurements while they are amplified in off-axis measurements.

One issue that exists when aligning wide FOV systems is the determination of how many field points should be measured. There is the need for both on-axis and off-axis measurements [4,5,6]. Ideally, a large number of field points should be measured, although measurement of the entire field is often challenging, time-consuming, and unrealistic. This brings the field sampling effect into play, and the imperative of determining the minimum number of field points to be measured, as well as their sampling distribution.

A reverse-search algorithm attempts to discover the misalignment of components by measurement of the system WFE at a specific number of field points. It then applies the theoretical Zernike sensitivity table to the misaligned parameters and the measured Zernike coefficients of the optical system under the disturbed alignment. This technique has been well developed and implemented in optical design software, such as Zemax and CODE V. [7,8] (For the work developed in this paper, Zemax OpticStudio 18.9 version was used.) If the variation of the WFE Zernike coefficients with the misalignment parameters is sufficiently linear, the technique affords relatively high accuracy and convergence to the unique misalignment state determined by reverse estimation. This “reverse” approach means that one must start with a misaligned state, sample the system, and use that as an input to create a misaligned model; subsequently applying the reversed optimized value into the system to correct the misalignment.

These Zernike coefficients are useful for expressing wavefront data because they are of the same form as the aberrations observed in optical tests. One of the useful features of a Zernike polynomial is that it has a simple rotational symmetry that allows its expression as a product of the radial term (ρ) and a function of the angle (θ) [9]. The Fringe Zernike scheme

is presented in Table 1 [10]. Often, only the first nine or sixteen terms are used because the lower-order terms provide sufficient insight into the misaligned optical system without the need to use the high-order terms (not included in Table 1). Additionally, due to the presence of the central obscuration on the telescope, the pupil mask on the grism also has a central obscuration. In this case it was determined that 16 Zernike fringe coefficients would sufficiently represent a measurement with a central obscuration. Please, note that the presented work does not require the orthogonality of the utilized Zernike polynomials. As long as a polynomial can sufficiently represent (i.e., fit) the measured (and simulated) wavefront for each field, the polynomial can be used. However, it is worth mentioning that a non-orthogonal case may require more terms to fully represent a wavefront, which may result in numerical calculation costs such as CPU time [11].

Is it also important to mention that the Zernike coefficients in Table 1 are orthonormal over a unit disk domain. The specifications for the grism are defined over a circular aperture, allowing for the measured wavefronts discussed in Section 5 to be acceptable.

In the present study, we extended a previously reported reverse optimization algorithm [6] that uses merit function (MF) regression instead of a sensitivity table, employing various weighting factors [2,6,12,13]. The proposed technique utilizes

MF minimization of the measured Zernike coefficients of the optical system. The regression process also utilizes the damped least squares method, which is a commonly used optimization algorithm in the Zemax raytracing software, through active adjustment of the selected misalignment parameters of the modeled optical system until the minimum MF value is obtained. We used the initially proposed technique to determine the best alignment state of the WFIRST grism system and verified the results by comparing them with those of the currently employed sensitivity table method.

Section 2 of this paper describes the optical characteristics of the WFIRST grism system. Section 3 presents the theoretical basis of the MF regression method and the field-dependent error sources. Section 4 describes some large-FOV simulations that were performed using various field samplings to determine the minimum number and distribution of measurement field points required for the alignment of a system with a large FOV similar to that of the WFIRST. The simulations included runs using the actual grism engineering development unit (EDU) model. Section 5 presents the results of the alignment simulation and experimental measurements to demonstrate the superior performance of the proposed MF regression method compared with the sensitivity table method used for alignment of the WFIRST grism. A summary of the study is finally presented in Section 6.

Table 1. Mathematical Representation of the First 16 Fringe Zernike Polynomials, Type of Aberration, and Graphical Expression [10]

Zernike Term	Mathematical Representation	Aberration	WFE Map
Z_1	1	Piston	
Z_2	$\rho \cos \theta$	Distortion/tilt	
Z_3	$\rho \sin \theta$		
Z_4	$2\rho^2 - 1$	Defocus/field curvature	
Z_5	$\rho^2 \cos 2\theta$	Primary astigmatism	
Z_6	$\rho^2 \sin 2\theta$		
Z_7	$(3\rho^3 - 2\rho) \cos \theta$	Primary coma	
Z_8	$(3\rho^3 - 2\rho) \sin \theta$		
Z_9	$6\rho^4 - 6\rho^2 + 1$	Primary spherical	
Z_{10}	$\rho^3 \cos 3\theta$	Elliptical coma (trefoil)	
Z_{11}	$\rho^3 \sin 3\theta$		
Z_{12}	$(4\rho^4 - 3\rho^2) \cos 2\theta$	Secondary astigmatism	
Z_{13}	$(4\rho^4 - 3\rho^2) \sin 2\theta$		
Z_{14}	$(10\rho^5 - 12\rho^3 + 3\rho) \cos \theta$	Secondary coma	
Z_{15}	$(10\rho^5 - 12\rho^3 + 3\rho) \sin \theta$		
Z_{16}	$20\rho^6 - 30\rho^4 + 12\rho^2 - 1$	Secondary spherical	

2. WFIRST GRISM SPECTROGRAPH

The WFIRST is a NASA observatory designed to perform wide-field imaging and slitless spectroscopic surveys of the near-infrared sky [14]. The observatory utilizes a 2.4 m diameter primary mirror, and its payload includes two main instruments, namely, a wide-field instrument [15–18] and a coronagraph [19,20]. The wide-field instrument enables wide-field imaging and slitless spectroscopic capability through the use of a grism. Figure 1 compares the WFIRST FOV with those of the James Webb Space Telescope (JWST) and Hubble Space Telescope (HST).

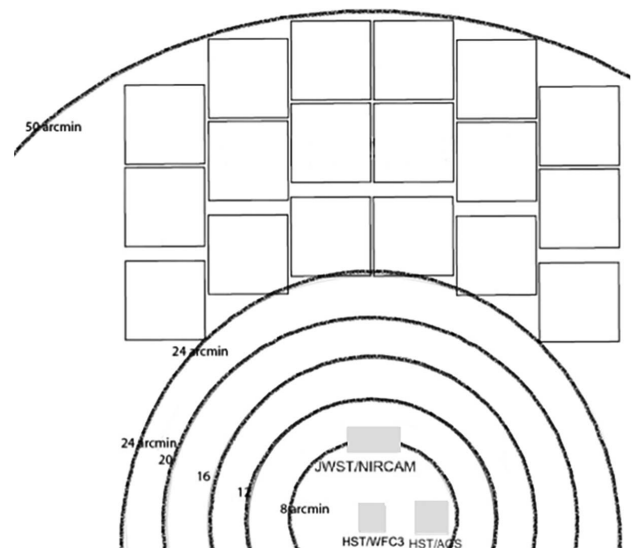


Fig. 1. Comparison of the field of view of different space telescopes [14].

WFIRST offers Hubble sensitivity and 0.1 arcsec resolution over a 0.28 square degrees field of view that is 100 times the field of HST's visible cameras. This highlights the WFIRST's optical and scientific capability mutually complementing the JWST and HST.

The WFIRST three-mirror anastigmat design is constrained and influenced by existing hardware/assets. However, the design allows for small changes in the conic figure of the primary mirror (T1) and minor changes in the curvature of the secondary mirror (T2). The tertiary is a powered mirror within the instrument (M3) that works in concert with T1 and T2 to correct the field across the focal plane array (FPA). All three powered mirrors are optically coaxial and simple conics. Two fold mirrors are used for packaging. Figure 2 shows the optical layout for the WFIRST wide-field instrument, where the pupil, located between M3 and the FPA, is the cold/Lyot stop and is located in front of the element wheel. This stop blocks the scatter and emissions from the telescope struts and baffles. The 11-position element wheel carries seven bandpass filters, an engineering filter, the grism system, the prism system, and one null position. All elements of the wheel are par-focal to the system [16].

The grism has been through multiple design cycles. In 2013, a compound grism was modeled, with the design including a prism-like optic surrounded by two diffractive plano-convex lenses. The design was used to build the grism prototype, which covered a spectral range of 1.35–1.95 μm [3,21]. In the latest design cycle effort, the need to cover an even larger 1.0–1.9 μm spectral range was introduced, changing the design and making it four elements. The grism EDU design consists of four optical elements, E1–E4, with an integrated Lyot stop. E1 and E4 are thin plane-parallel plates containing binary diffractive optical elements that balance the dispersion and aberration of the system. The gratings are etched onto only one of the surfaces of the diffractive elements. E2 and E3 are powered prism elements with wedges and have only spherical surfaces similar to meniscus lenses. E1 is mounted on the baseplate, referred to as the grism deck, while E2–E4 are mounted in succession on the grism deck in their respective mounts. The position of each element in its mount can be adjusted through spherical washers that allow six degrees of freedom (DOFs) adjustment. Figure 3 shows a side view of the grism optical model, its computer-aided design (CAD) model, and the actual assembled grism instrument.

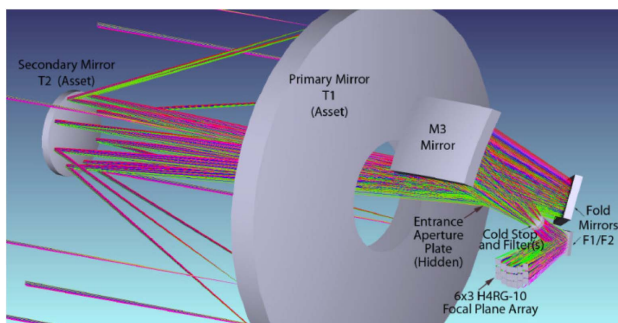


Fig. 2. Optical layout of the WFIRST wide-field instrument [16].

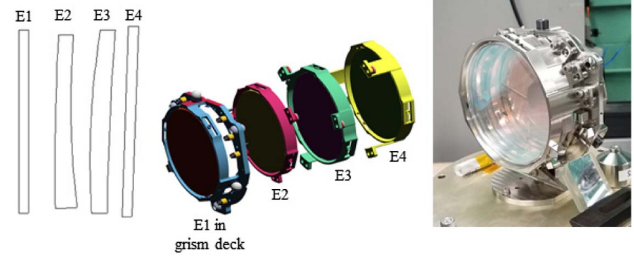


Fig. 3. Grism engineering development unit. From left to right: optical model, CAD model, and assembled grism instrument, where E1 and E4 contain the diffractive optical elements.

The WFE of the grism is within values that afford satisfactory diffraction-limited performance across the entire spectral range of the system. The main challenge of the optical design is the wide FOV, high dispersion, relatively small f -number, and the difficulty of fabricating the required high-efficiency diffractive surfaces. Table 2 gives the EDU specifications, and Fig. 4 shows the nominal design residual WFE RMS performance of the grism, where each square represents a detector on the focal plane array.

Table 2. WFIRST Grism EDU Specifications

Wavelength range (μm)	1.0–1.9
WFIRST FOV (deg)	0.75×0.383
Average beam diameter at grism (mm)	100
Beam f -ratio at grism (mm)	$\sim f/8$
Wavefront error	Diffraction limited at $\lambda > 1.0 \mu\text{m}$
Spectral resolution	435–856
Capability	Dispersion and pointing for spectrometer
Compactness	~ 80 mm total thickness for a fixed diameter ~ 120 mm
Beam deviation	Zero at 1.55 μm

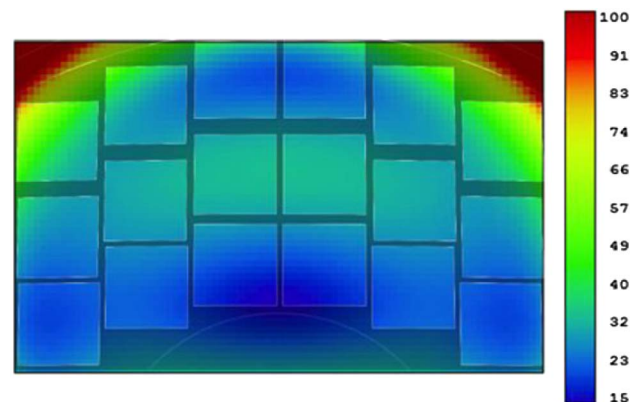


Fig. 4. Nominal design residual WFE RMS performance of grism EDU at 1.55 μm on the FPA. The unit of the scale is nm [21].

3. MULTI-FIELD MERIT FUNCTION REGRESSION METHOD

A. Multi-Field Merit Function Regression Method for Non-Symmetric Systems

The objective of aligning any optical system, be it a symmetrical or non-symmetrical one, is to minimize the aberrations in the system and obtain the best possible performance of the entire focal plane. Experimentally, this has been conventionally accomplished by using an interferometer to measure the WFE RMS values for various field points that best represent the full field of the system. A compensator is then used to minimize the aberrations in the system. Such a compensator should be capable of perturbations corresponding to the various DOFs of the system: XY decentering translation, θ_x, θ_y tipping and tilting, θ_z clocking, and Z axial translation along the optical axis.

There are established relationships between some adjustments and aberrations such as transverse aberrations, which include astigmatism and coma, known to be coupled with decentering and tilting; and unlike longitudinal aberrations such as defocus and spherical, which are mostly coupled with despacing. More detailed versions of such relationships can be obtained for any system by conducting a sensitivity analysis. This enables observation of the WFE at any field point set by a combination of Zernike coefficients.

If it is assumed that the Zernike coefficients are linearly related to the misalignments, then each coefficient can be derived from a linear combination of the different misalignment parameters, with each having its own relevant sensitivities per field point. This can be expressed as $\Delta Z = A\Delta D$ [5,12,13], where

$$\Delta Z = \begin{bmatrix} \Delta Z_1 \\ \vdots \\ \Delta Z_m \end{bmatrix} = \begin{bmatrix} Z_1 \\ \vdots \\ Z_m \end{bmatrix} - \begin{bmatrix} Z_{1o} \\ \vdots \\ Z_{mo} \end{bmatrix},$$

$$A = \begin{matrix} \frac{\partial Z_1}{\partial x_1} & \dots & \frac{\partial Z_1}{\partial x_n} \\ \vdots & & \vdots \\ \frac{\partial Z_m}{\partial x_1} & \dots & \frac{\partial Z_m}{\partial x_n} \end{matrix}, \text{ and}$$

$$\Delta D = \begin{bmatrix} \Delta x_1 \\ \vdots \\ \Delta x_n \end{bmatrix} = \begin{bmatrix} x_1 \\ \vdots \\ x_n \end{bmatrix} - \begin{bmatrix} x_{1o} \\ \vdots \\ x_{no} \end{bmatrix}. \tag{1}$$

Here, ΔZ is the difference between the measured and modeled Zernike coefficients; A is the sensitivity table obtained from the nominal model; and ΔD is the sum of the disturbances or compensators of the alignment parameters x_i , such as the XYZ and tilt (θ_{xyz}) displacements; and m and n are the total number of Zernike coefficients and the total number of alignment parameters, respectively.

This method affords a highly accurate estimation of the misalignment parameters as long as the linear relation between the Zernike coefficient sensitivity and the alignment perturbation is maintained [6,13]. If the system is significantly misaligned, the resulting non-linearity of the Zernike sensitivity would considerably affect the residual error of the method. Additionally, the fact that the nominal model is used to generate the sensitivity

table (A) may further aggravate the problem because the measured coefficients that contain field errors would increase the sources of the residual error.

In Zemax the MF is defined as the sum of the various field components. In the present case, it is the sum of the errors of the different field components, with sixteen Zernike terms (see Table 1) at each field point

$$MF^2 = \frac{\sum W_{(f,Z)}(V_{(f,Z)} - T_{(f,Z)})^2}{\sum W_{(f,Z)}}, \tag{2}$$

where V and T are the current and target values of the selected parameters, respectively; f represents the various field components; Z represents the first sixteen Fringe Zernike coefficients for each field; and W is the weighting factor of each term. In most commercial optical design software, the actively damped least square method is used to minimize the MF value and obtain the best-fit parameters.

The MF regression method for the full field of a system requires the initial determination of the first sixteen Fringe Zernike coefficients from interferometric measurements. Here, $T(f, Z)$ represents the misaligned state of the system. The ideal or nominal model Fringe Zernike coefficients are then assigned to $V(f, Z)$, which represents the nominal alignment status of the optical system. Subsequently, the measured coefficients are assigned to $T(f, Z)$ (measured values inputted to the “target” column of the Merit Function Editor), and a weighting factor of unity is set for all the variables. This is followed by running the optimization algorithm (using, for example, the damped least square technique) embedded in the software to minimize the MF. This allows the variation (optimization) of the alignment parameters, which are selected by the user as the variables, so that $V(f, Z)$ approaches $T(f, Z)$ as closely as possible. When a minimized MF is obtained, the outputs are the alignment parameters, which indicate the current misalignment state of the measured optical system. This optimization approach has been previously used by others [5,6,7,13], but the specifics of this algorithm (inputs and outputs) are particular to the system discussed in this paper.

Sixteen Fringe Zernike coefficients for each field sampling point are inputted into the MF for the presented case. Depending on the test configuration, additional coefficients may be desirable. For instance, for the four field sampling case, there are total $(16 \times 4 =)64$ Zernike coefficients representing the current alignment status of the optical system guiding the optical modeling software to search the current misalignment state in terms of the given alignment terms. We acknowledge that there might be a case with degeneracy issue, which depends on the optical design specifics and the as-manufactured alignment terms. The general approach utilizing the raytracing software to address the practical complexity of given optical systems, however, is still valid.

B. Error Sources: Field Sampling, Positioning, and Others

Ideally, in the measurement of the WFE for a specific field angle, the reference spherical wave from the interferometer should be focused on the exact field position relative to the focal plane of the telescope. However, in reality, identification of the correct field position at the telescope level is difficult and usually

involves a residual positioning error. This error constitutes an estimation error source for the given alignment state in the sensitivity table method. A previous study [6] has shown that the MF value approaches nearly zero at ± 0.02 deg from the on-axis field point, indicating that the MF regression method can be used to determine the shifted field position being sought for and is thus very useful for computing the field positioning error.

Another field-associated error is related to sampling when measurement of the full field is ideal but only a few field points can be practically measured due to time and space constraints. In this case, the determination of the appropriate number of measurements can be difficult. The following section describes a simulation process that was used to address this issue.

Other sources of error include the environmental interferometric testing conditions. For example, if the interferometer is exposed to turbulent conditions and the setup does not include a floating table, vibration may come into play, decreasing the measurement repeatability to a lower level of 3–4 nm RMS compared with the normal level of 1 nm or less RMS.

4. SIMULATION STUDY OF THE FIELD SAMPLING EFFECT

When attempting to determine the number of field points required to align a wide-field system, the measurement of one on-axis field point does not yield sufficient information to obtain insight into the full field performance [4,5]. If only one on-axis field point is measured, the results would certainly indicate misalignment, but it could also be due to manufacturing errors and even setup disturbances because the various contributors cannot be independently isolated by a single measurement.

Figure 5 shows the footprint and spot diagrams of the nominal grism EDU assembly for 18 field points, one per detector (as shown in Fig. 4). The spot diagrams are similarly positioned (vertically and horizontally) to the corresponding points in the footprint diagram and the detector positions.

The following simulation results verify that a manufacturing error could be confused and interpreted as a misalignment. The simulation assumed that the nominal model was perturbed within the alignment tolerances if only the on-axis Fringe Zernike coefficients were sampled and used to simulate the same performance but the E2 and E3 surface figures could be perturbed to simulate a manufacturing error. In practice, these uncertainties can be minimized or eliminated by component-level quality control. Under these conditions, both models would produce the same Zernike coefficients on-axis but for different reasons. This indicates that the same Zernike coefficients can result from misalignment and/or a specific surface shape error (i.e., manufacturing error). Figure 5 compares the spot diagram obtained when using on-axis and 18 field points (one per detector) as the input to optimize the alignment performance of a system by the MF regression method. Expectedly, when more fields were measured, the model yielded better results for the full field. The spot diagram aligned using 18 field points as input shows most spot diagrams to be successfully diffraction limited (Fig. 5 bottom), unlike the case of on-axis single input in which there was a fewer number of diffraction-limited spots (Fig. 5 top).

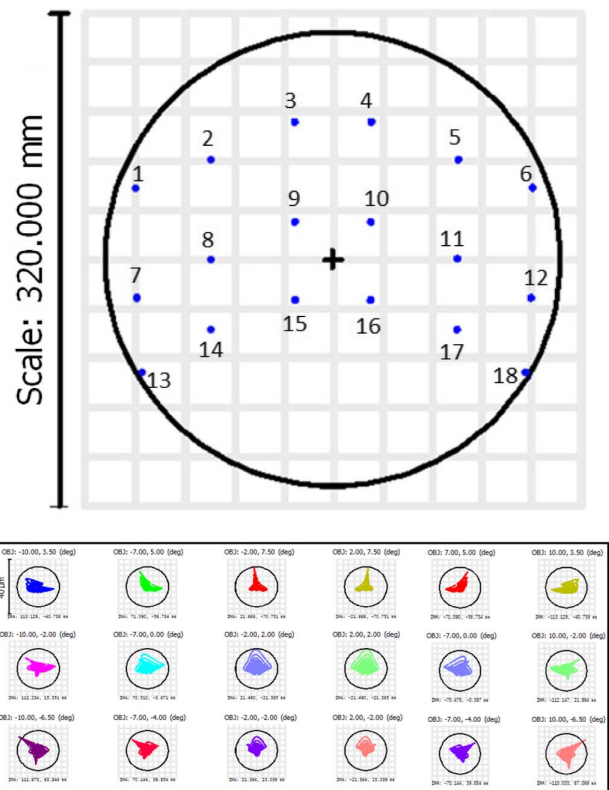


Fig. 5. Footprint diagram (top) and spot diagram with an Airy disk circle of $14.59 \mu\text{m}$ radius (bottom) of 18 nominal field points for the WFIRST grism EDU. The full field distribution has a root sum squared (RSS) of 506 mm from the center of the field. Note that the field angles are in the grism coordinate frame, which is different from the WFIRST telescope FOV in Table 1.

For these types of measurements and/or simulations, it is important to know the minimum number of field points that should be inputted to the model to obtain the best possible performance from the alignment. Figure 6 clearly indicates the need for more than one field point, and while it is always desirable to measure most of the FOV for any system, this is often time-consuming and not always practical. Figure 7 shows the results of various simulations of both a grism EDU system and a grism-like system. In both cases, random errors were assumed to be present in the system, such as random measurement error, surface shape error, and misalignment, all which could be realistically impact the measured wavefront data quality and the finally aligned optical system performance. With these assumptions, the Zernike coefficients of the on-axis field point were first collected in the simulations, and used to optimize the alignment configuration. This was performed 10 times, with another field point added to the input each successive time. The results suggested the use of a minimum of four sampled measurement field points for the alignment of a large FOV instrument in the presence of all the actual uncertainties and noise. The plotted results indicated that the use of only one on-axis field point for the optimization may generate an aligned system for the on-axis imaging, but increasing the number of sampled field points would decrease the overall field WFE

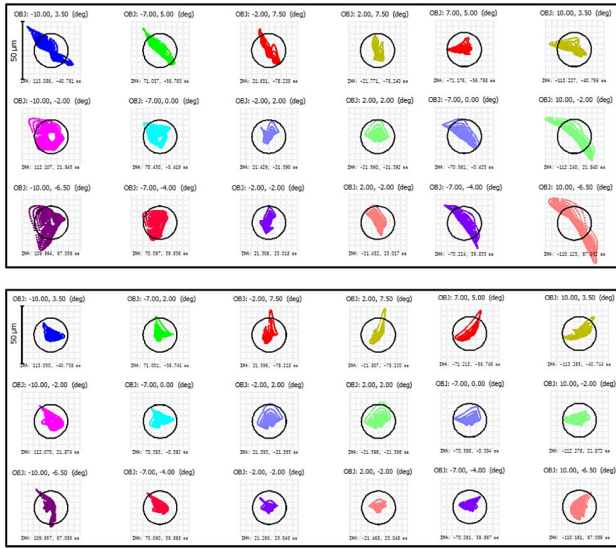


Fig. 6. WFIRST grism EDU spot diagrams performance comparison obtained using on-axis only (top) and 18 field points (bottom) as input. Note that the field angles are in the grism coordinate frame, which is different from the WFIRST telescope FOV in Table 1.

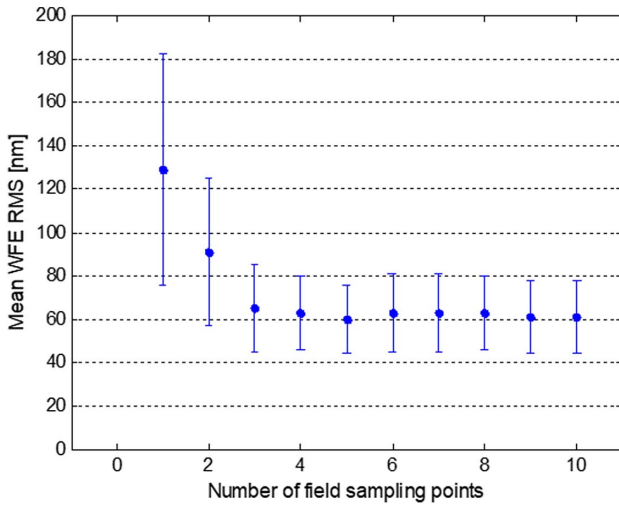


Fig. 7. Mean WFE RMS versus the number of field sampling points for the MF regression method input. The error bar represents the $\pm 1\sigma$ standard deviation.

RMS, and the use of more than four field points barely impacted the alignment. Even when the number of field points inputted to the model increased to 10, the WFE RMS remained the same. This highlights the importance of optimal (instead of a naive minimum or maximum) field sampling during the actual alignment of a wide FOV optical system. It must be noted that after four field points are used as an input, the error bars also seem to remain unaffected by the additional field points. This is consistent with the findings presented in Fig. 7. The WFE RMS barely changes after four field points and neither does its variation since the optical performance is now approaching the nominal design value balancing the overall field performance for a given merit function.

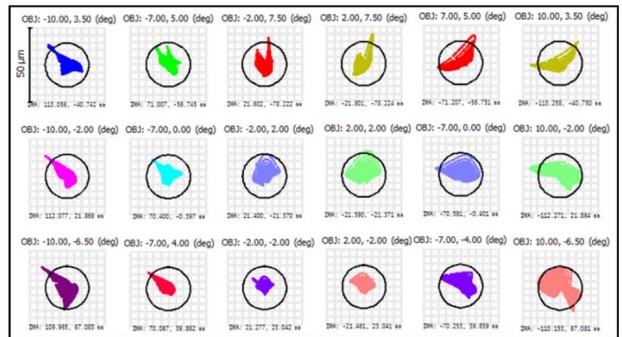
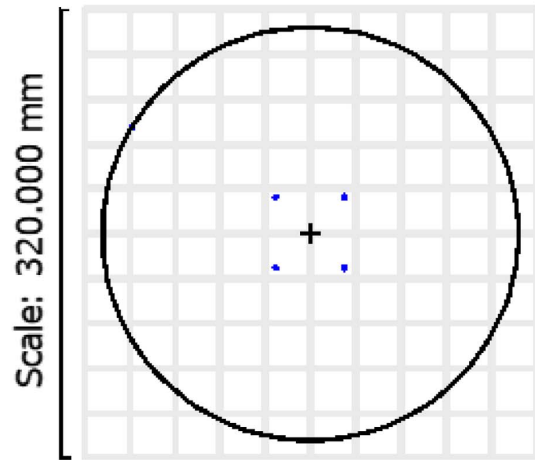
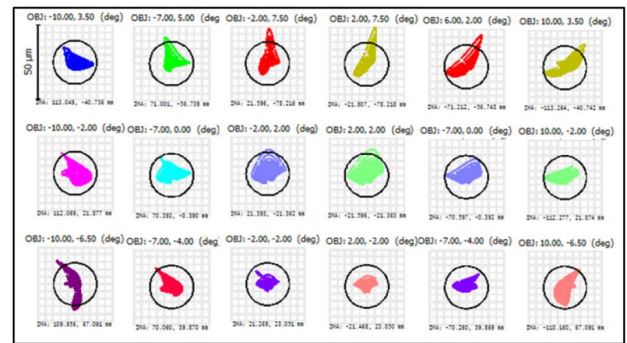
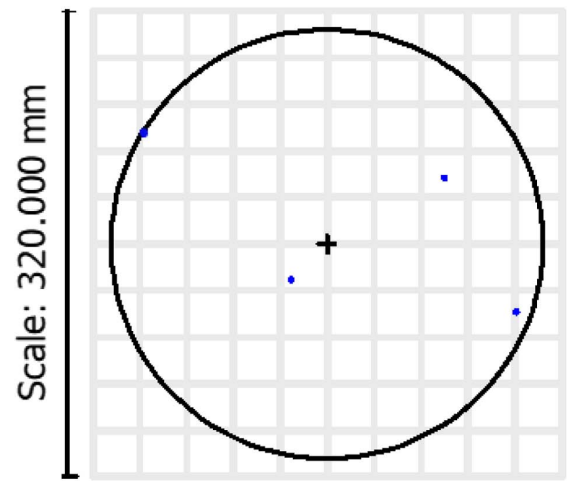


Fig. 8. (Continued)

Fig. 8. Comparison of two different sampling distributions using the MF regression method. For each sampling distribution, the top footprint diagram shows the selected field points and the bottom grid shows the spot diagram achieved after aligning the system using the MF regression method. The WFE RMS after alignment is distribution dependent. The distribution of the fields in the first case has an RSS of 268 mm and in the second case of 76 mm from the center of the field. Note that the field angles are in the grism coordinate frame, which is different from the WFIRST telescope FOV in Table 1.

As another case study, other simulations were run using the same number of field points (four) as the MF regression method input but with different sampling distributions. In one model, only central region field points were inputted (field points 9, 10, 15, and 16 from Fig. 5 top), and in another, only edge field points were inputted (field points 1, 15, 5, and 18 from Fig. 5 top). The results indicated that both of these models could converge to obtain an alignment solution. However, the model to which a combination of central and edge field points of the FOV were inputted produced a more accurate alignment solution, yielding a smaller WFE RMS across the full field. This suggests that better results can be obtained by sampling a larger portion of the field even if only four points are used, rather than only the central or on-axis section of the FOV, as shown in Fig. 8.

Figure 8 compares the spot diagrams for two different distributions of four inputted field points. The footprint diagram for the wider FOV (field points 1, 15, 5, and 18 from Fig. 5 top) has a corresponding set of spot diagrams with lower WFE RMS values across the full field, the average being 63 nm. In contrast, the average WFE RMS value for the smaller distribution (field points 9, 10, 15, and 16 from Fig. 5 top) is 71 nm. Furthermore, the spot diagram reveals a higher number of diffraction-limited spot diagrams when the sampling distribution is over a larger FOV when using the MF regression method. The footprint diagram in Fig. 8 shows the fields selected as input for the alignment optimization and the identical 18 field locations' spot diagrams (same as Fig. 5) are presented to objectively evaluate/compare the final aligned optical system's performance. A wider sampling distribution generates a smaller WFE RMS across the full field. We note that the performance comparison between the simulated two cases may depend on a given specific optical design/configuration. For instance, some optical design may have less or more wavefront variation characteristics as a function of field sampling distribution. Each optical system needs to be modeled and simulated in order to provide an optimal field sampling distribution, while this manuscript provides a general description of the approach.

5. WFIRST GRISM EDU ALIGNMENT USING THE MULTI-FIELD MF REGRESSION METHOD

A. WFIRST Grism EDU Alignment Setup

As mentioned in Section 2, the individual grism elements were fabricated with alignment fiducials written on the optics and integral flats polished on their sides to allow for opto-mechanical alignment with six DOFs. Each element was installed on a hexapod and positioned in its nominal orientation relative to the

grism deck (Fig. 3). Each element was separately first placed on the hexapod and theodolites were used to measure it to set the tip/tilt, while a Micro-Vu non-contact multisensor measurement system was used to set the spacing between the parts, decenter, and clocking, as shown in Fig. 9. All the measurements were relative to the grism deck, which was mounted on a ground support equipment bond fixture.

The adjustment of the various DOFs was enabled by the hexapod, which allowed the bonding of one optic at a time. The step size adjustment for the hexapod was $0.5 \pm 0.3 \mu\text{m}$ in the X and Y directions and $0.2 \pm 0.1 \mu\text{m}$ in the Z direction. The tip and tilt adjustments of the hexapod were respectively 3.5 ± 4 and $3.5 \pm 8 \mu\text{rad}$ for clocking (about Z) [22]. These fine adjustments enabled precise placement of the grism elements in their mechanical cells. Therefore, once the full assembly was mounted, all the optics were positioned within the allowable tolerances relative to the grism deck: $<20 \mu\text{m}$ for XYZ translation and $<45 \mu\text{rad}$ (~ 9 arcsec) for tip, tilt, and clocking. This was important because it allowed the assembly of the grism EDU to be well characterized so that any required adjustment after the measurement of the wide FOV could be easily accommodated. However, any such adjustments would be small, given the substantial effort that had been made to position the optics in their nominal position. Figure 9 shows the grism assembly held by the mini hexapod and bond fixture, with the entire unit placed under the Micro-Vu system in a cleanroom environment during assembly.

After completing the opto-mechanical alignment and bonding, the grism EDU was placed on a large hexapod in front of an infrared Zygo interferometer with a 6 in. $f/7.2$ IR transmission sphere and an operating wavelength of $1.55 \mu\text{m}$ to make it suitable for testing the grism, which had a design wavelength

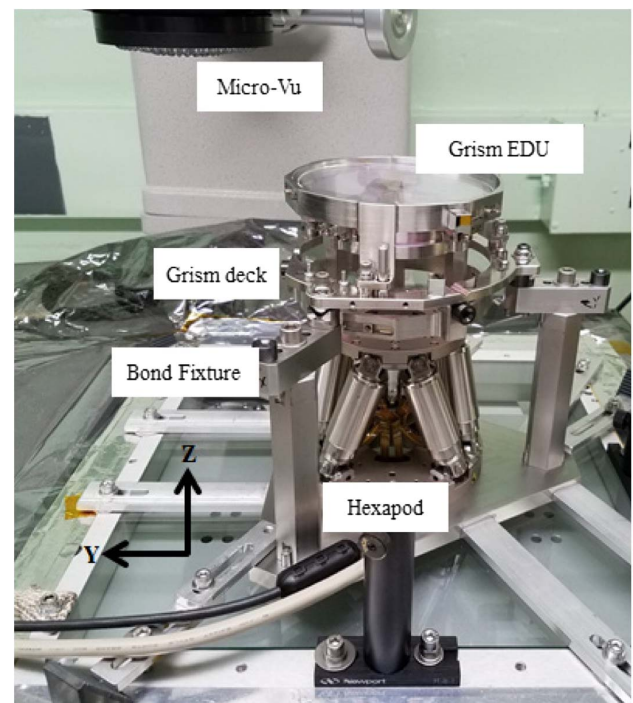


Fig. 9. Fully bonded WFIRST grism EDU on a hexapod under the Micro-Vu measurement system.

range of 1.0–1.9 μm . It is important to note that this test configuration does not precisely represent the actual setup of the grism in the WFIRST telescope. In the telescope, the source is moveable while the grism remains fixed; see the sketch in Fig. 10(a) (note that this figure shows an oversized detector plane; it is just a sketch to show the difference between the test setup in the lab for the results presented and that which will be implemented in the future). However, in the present test, the grism was moveable while the source (the interferometer) remained fixed. There were multiple reasons for the present test setup. (1) First, it should be noted that further tests are planned, which will utilize a movable source and cover the entire waveband of the grism; (2) it was preferable in the present test not to move the interferometer each time a new measurement was to be made; and (3) the hexapod allowed for a very precise DOF adjustment of the grism [23].

Several field points were measured on the grism, extending over a 20×14 deg FOV for the local grism coordinate system, measured relative to the grism pupil. Section 4 indicates that only four field points are needed when using the multi-field MF regression method; however, seven field points were measured for redundancy purposes considering the non-modeled uncertainties and other error sources.

Figure 10(b) shows the test setup in the laboratory, including the various metrology instruments used, such as the infrared interferometer, laser tracker, hexapod, and micrometer digital display XYZ stage. A spherically mounted retroreflector (SMR) was placed at the interferometer focus so that the laser tracker could measure its position along with various other targets located on the grism deck that were used as tie points for monitoring and ensuring that the translational displacements between the grism and the focus were the same for all the field points, as is the case in the telescope.

B. Wavefront Sampling Distribution for Grism EDU Alignment

The grism EDU wavefront error was measured at seven different field points selected to represent the edges of the WFIRST

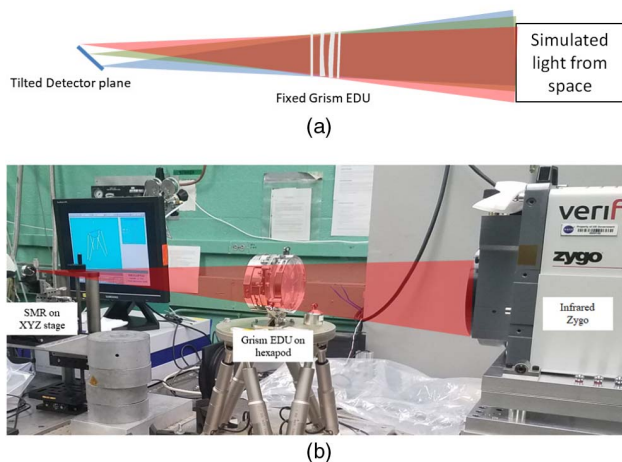


Fig. 10. (a) Sketch of the grism being tested in the future, with a movable source and a fixed grism EDU, where the detector plane is exaggerated in size to dramatize the difference between setups. (b) Grism EDU on hexapod, in front of an infrared interferometer to measure WFE at various field points. The red cone illustrates the infrared beam emitted by the interferometer.

FOV, as shown in Figs. 4 and 11. The hexapod allowed the placement of the grism relative to the interferometer and its focus. The initial on-axis distance between the grism deck plane and the interferometer focus was 725.054 ± 0.025 mm, with further adjustments made for focus over the entire duration of the measurements. The on-axis (0,0) field point measurement was recorded when the grism was normal to the interferometer beam. Figure 11 shows the measured seven field positions and their distribution on the FPA of the WFIRST telescope.

As would be expected for any complex, non-symmetrical system, it was observed after completion of the first set of measurements that the measured WFE at any of the field points did not meet the requirements, with the results being particularly poor at the edge of the field. It must be borne in mind that the repeatability of the WFE measurement was approximately 4% of the interferometrically measured value, due to various unstable laboratory conditions, coupled with the fact that the interferometer was placed on an optical table that was not floating (note: this table was selected because it holds the cryogenic chamber that will be used to test the grism environmentally; however, the table cannot float because of the mounting of the cryogenic heads needed to run the chamber), owing to experimental limitations.

The first alignment correction was attempted using modeled alignment sensitivities (sensitivity table method). It was decided that only E2 would be used as a compensator because it was the thickest element and sensitivity studies have shown that such optics could best be used to correct the power and astigmatism terms of the entire system by adjusting its spacing and tip/tilt. This is unlike the case of other grism optics, which have Zernike terms that are more coupled and the adjustment of one DOF would significantly perturb the other terms. Additionally, the adjustment of only one element in the present case enabled better adjustment control. The alignment sensitivities indicated that E2 could be successfully used to minimize the field-dependent WFE and confocality under ambient and cryogenic

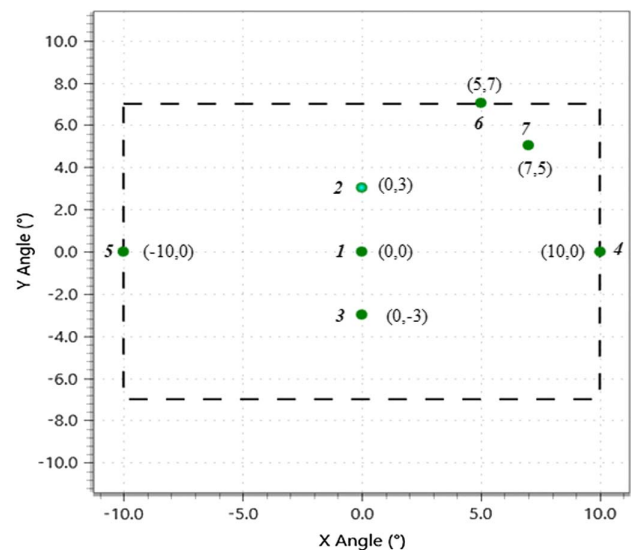


Fig. 11. Number and position of the measured seven field points of the WFIRST grism EDU alignment using the multi-field MF regression method.

conditions. This paper discusses only the measurements under ambient conditions; those under cryogenic conditions are ongoing and will be reported at a later time.

Multiple alignment attempts were made after the first measurement, during which only E2 was adjusted with three DOFs: spacing (Δz), tip (θ_x), and tilt (θ_y). Clocking (θ_z) and X and Y decenter translations of E2 were controlled by bushings, which fixed E2 relative to the grism deck. Adjustment of the X and Y decenter translations were avoided because of the difficulty of controlling them.

The tip, tilt, and spacing adjustments could be easily and accurately measured using theodolites and micrometer gauges, including the thickness of the shims used to adjust the tip and tilt. However, the clocking control was relatively imprecise because clocking could more easily combine with XY displacement and could change when torquing the bolts that hold the grism.

After completion of the various adjustments using the sensitivity table method, an alignment that met the requirements was obtained as presented in Table 3. Alignment sensitivity tables were used for the entire process because an attempt had not yet been made to apply the MF regression method. The employed MF regression method was only applied after the known required adjustments had been made, with the initial WFE measurements across the field used as input. This represented a type of “reverse engineering” approach and was successfully demonstrated and confirmed by optimizing the alignment using the multi-field MF regression process and comparing the optimized results with the initial measurements, as described in Section 5.C and Table 3.

As mentioned in Section 3 that the Zernike coefficients are linear to misalignments, each Zernike coefficient can be derived from the linear combination of the various misalignment parameters with relevant Zernike sensitivities. ΔZ is the difference of Zernike coefficients between the measurement data and the nominal design, and A is the Zernike sensitivity table (see Section 3). As shown in other publications [1,5,12], the sensitivity table method showed high accuracy in finding misalignment parameters in simulations. Yet, this method is based on the linearity of the Zernike sensitivities. It would be valid only if the misalignments of each parameter are located around the nominal positions. If the misalignment parameters are not sufficiently linear or one or more misalignment parameters are coupled to one another, the method could be inefficient; the sensitivity method could give larger error and several iterations would be needed to reach to the nominal positions.

Figure 12 shows the plotted numbers listed in Table 3. We acknowledge that not all the WFE RMS values measured and reported in Table 3 match those estimated by the multi-field MF regression method. This is partly due to a large error associated with the E2 and E3 measured spacing using the Micro-Vu instrument.

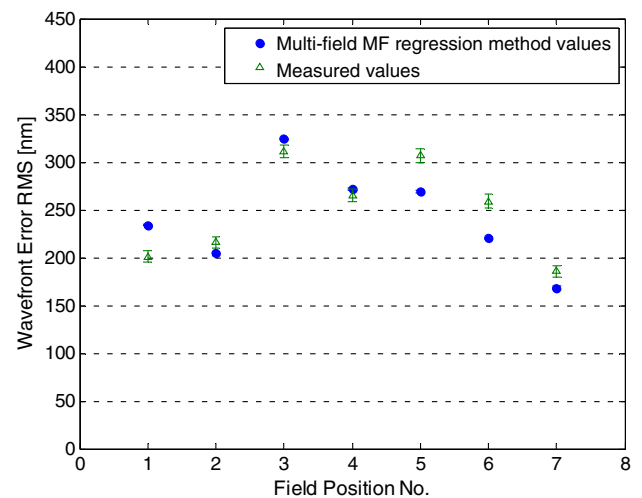


Fig. 12. Comparison of the WFIRST grism EDU measured and optimized WFE RMS for each field point. The error bar represents the $\pm 1\sigma$ standard deviation.

C. WFIRST Grism EDU Final Alignment Performance using Multi-Field MF Regression Method

After the achievement of the required wavefront performance by the alignment sensitivity table method, an MF was created using the multi-field MF regression method by inputting the measured Fringe Zernike coefficients (4–16) for each field point, with all the Zernike coefficients having equal weight. An additional constraint was used to restrict the range of each of the optimized variables so that the system would make reasonably optimized adjustments of the E2 despace, tip, and tilt.

Table 4 compares the adjustments measured by theodolites (tip, tilt, and clocking of the alignment cubes), micrometer gauges (shim thickness), and the Micro-Vu measurement system (focus) with those calculated by the multi-field MF regression method. Although the Δz adjustment does not match the optimized value, it is in reasonable agreement; its large error originates from issues related to measurement of its alignment fiducial using the Micro-Vu instrument. All the other angle

Table 4. Comparison between the Measured E2 Adjustments and Those Calculated by the Multi-Field MF Regression Model

E2 DOF Adjustment	Measured with Theodolite/Micrometer	Multi-Field MF Regression Method Modeled
E2-E3 Z-space (Δz) [μm]	323 ± 75	407.2 ± 2.3
E2 tilt about X (θ_x) [deg]	-0.190 ± 0.025	-0.187 ± 0.002
E2 tilt about Y (θ_y) [deg]	0.110 ± 0.025	0.124 ± 0.0004
E2 clocking about Z [deg]	0.040 ± 0.034	0 ± 0.0

Table 3. Comparison between the Measured and Multi-Field MF Regression Calculated WFE RMS

Field Position No.	1	2	3	4	5	6	7
Measured WFE RMS [nm]	201 ± 6	216 ± 6	311 ± 7	265 ± 7	307 ± 7	259 ± 7	186 ± 6
Multi-field MF calculated WFE RMS [nm]	234 ± 1	204 ± 2	324 ± 1	272 ± 1	269 ± 1	220 ± 1	168 ± 2

adjustments are within their error uncertainties, indicating that the MF regression method successfully predicted the necessary adjustments for improving the grism alignment to meet the requirements. The errors of the MF regression method are related to the repeatability of the WFE measurement.

While the E2 adjustments mostly match those estimated by the multi-field MF regression method within the error limits, we acknowledge that the respective WFE RMS values presented in Tables 3 and 4 and Fig. 12 are also only comparable and not exactly equal. The large errors of the measured spacing between E2 and E3 presented in Table 4 contribute to the discrepancies because measurement of the spacing between the coated optics using the Micro-Vu system was difficult, generating a large error along the Z -axis. Other contributors to the discrepancies are surface shape errors, misalignment of other elements, and measurement errors.

The sensitivity table method used initially to align the grism EDU was successful, but it required seven time-consuming iterations. In the case of the presented and cross-confirmed multi-field MF regression method, once the model was correctly set up, calculating the required E2 adjustments only required running the numerical model for an accurate optimization. This substantiates the superiority of the multi-field MF regression method with regard to accuracy, speed, and ease of use.

6. SUMMARY

Through an examination of the field sampling effect, we successfully presented and validated the use of the multi-field MF regression method for a wide FOV optical system alignment. It is worth noting that there might be some cases with degeneracy issues, which may limit the use of presented numerical optimization approach, for a given specific optical system with as-built alignment terms.

The method utilizes an MF consisting of Fringe Zernike coefficients that represent the misaligned system and attempts to minimize the MF to estimate the misalignment state using actively damped least square algorithms. The results of simulations and case study experiments confirmed that the method was more effective and accurate than the conventional Zernike coefficient sensitivity table method. This is particularly the case when the field sampling effect is considered, with a minimum number of four field points required for adequate sampling of a large FOV. Seven field points were sampled in the present work, in which the multi-field MF regression method was specifically used to verify the alignment of the WFIRST grism EDU instrument under ambient conditions. We believe that, with the use of the required distribution of the field sampling points, the method can be used to achieve better convergence in the alignment of a wide range of optical systems.

Acknowledgment. We thank Jason Krom and Patrick Williams for their design of the mechanical housing of the grism instrument employed in this study and their assistance in the alignment process. We are also grateful to Joseph McMann for his invaluable support with the collection of the experimental data.

REFERENCES

1. E. D. Kim, Y.-W. Choi, M.-S. Kang, and S. C. Choi, "Reverse-optimization alignment algorithm using Zernike sensitivity," *J. Opt. Soc. Korea* **9**, 68–73 (2005).
2. M. A. Lundgren and W. L. Wolfe, "Simultaneous alignment and multiple surface figure testing of optical system components via wavefront aberration measurement and reverse optimization," *Proc. SPIE* **1354**, 533–539 (1991).
3. Q. Gong, D. Content, J. Kruk, B. Pasquale, T. Wallace, and W. Smith, "Design, fabrication, and test of WFIRST/AFTA grism assembly," in *Classical Optics*, OSA Technical Digest (online) (Optical Society of America, 2014), paper IM3A.5.
4. H.-S. Yang, Y.-W. Lee, E. D. Kim, Y.-W. Choi, and Ad. A. Ad. Rasheed, "Alignment methods for Cassegrain and RC telescope with wide field of view," *Proc. SPIE* **5528**, 334–341 (2004).
5. B. Zhang, X. Zhang, C. Wang, and C. Han, "Computer-aided alignment of the complex optical system," *Proc. SPIE* **4231**, 67–72 (2000).
6. S. Kim, H.-S. Yang, Y.-W. Lee, and S.-W. Kim, "Merit function regression method for efficient alignment control of two-mirror optical systems," *Opt. Express* **15**, 5059–5068 (2007).
7. R. Melich, P. Psota, V. Ledl, and J. Vaclavik, "Irregular surfaces—measurements and ZEMAX simulations," *Eur. Phys. J.* **48**, 00015 (2013).
8. Synopsys, <https://www.synopsys.com/optical-solutions/codev/features.html>.
9. E. P. Goodwin and J. C. Wyant, *Field Guide to Interferometric Optical Testing* (SPIE, 2006).
10. J. Schwiegerling, "Review of Zernike polynomials and their use in describing the impact of misalignment in optical systems," College of Optical Sciences, Faculty homepage for Jose Sasian, 2018, <https://wp.optics.arizona.edu/jsasian/wp-content/uploads/sites/33/2018/04/Schwiegerling-Zernike-2018.pdf>.
11. M. Aftab, J. H. Burge, G. A. Smith, L. Graves, C. Oh, and D.-W. Kim, "Modal data processing for high resolution deflectometry," *Int. J. Precis. Eng. Manuf.-Green Tech.* **6**, 255–270 (2019).
12. H.-S. Yang, S.-H. Kim, Y.-W. Lee, J.-B. Song, H.-G. Rhee, H.-Y. Lee, J.-H. Lee, I.-W. Lee, and S.-W. Kim, "Computer aided alignment using Zernike coefficients," *Proc. SPIE* **6293**, 62930I (2006).
13. Y. Kim, H.-S. Yang, S.-W. Kim, and Y.-W. Lee, "Alignment of off-axis optical system with multi mirrors using derivative of Zernike polynomial coefficient," *Proc. SPIE* **7433**, 74330C (2009).
14. B. A. Pasquale, C. T. Marx, G. Gao, and N. Armani, "Optical design of the WFIRST phase-A wide field instrument," in *Optical Design and Fabrication (Freeform, IODC, OFT)*, OSA Technical Digest (online) (Optical Society of America, 2017), paper ITh1B.2.
15. B. J. Holler, S. N. Milam, J. M. Bauer, C. Alcock, M. T. Bannister, G. L. Bjoraker, D. Bodewits, A. S. Bosh, M. W. Buie, T. L. Farnham, N. Haghhighipour, P. S. Hardersen, A. W. Harris, C. M. Hirata, H. H. Hsieh, M. S. P. Kelley, M. M. Knight, E. A. Kramer, A. Longobardo, C. A. Nixon, E. Palomba, S. Protopapa, L. C. Quick, D. Ragozzine, V. Reddy, J. D. Rhodes, A. S. Rivkin, G. Sarid, A. A. Sickafoose, A. A. Simon, C. A. Thomas, D. E. Trilling, and R. A. West, "Solar system science with the Wide-Field Infrared Survey Telescope," *J. Astron. Telesc. Instrum. Syst.* **4**, 034003 (2018).
16. B. Pasquale, D. Content, J. Kruk, D. Vaughnn, Q. Gong, J. Howard, A. Jurling, E. Mentzell, N. Armani, and G. Kuan, "Optical design of WFIRST-AFTA wide-field instrument," in *Classical Optics*, OSA Technical Digest (online) (Optical Society of America, 2014), paper IM3A.7.
17. B. A. Pasquale, T. Casey, C. Marx, G. Gao, N. Armani, D. Content, J. Hagopian, A. Jurling, C. Jackson, A. Liu, A. Whipple, and J. Murray, "Optical design and predicted performance of the WFIRST phase-b imaging optics assembly and wide field instrument," *Proc. SPIE* **10745**, 107450K (2018).
18. B. A. Pasquale, D. Content, J. Kruk, D. Vaughnn, Q. Gong, J. Howard, A. Jurling, L. Seals, E. Mentzell, N. Armani, and G. Kuan, "Optical design of the WFIRST-AFTA wide-field instrument," *Proc. SPIE* **9293**, 929305 (2014).
19. J. Krist, R. Effinger, B. Kern, M. Mandic, J. McGuire, D. Moody, P. Morrissey, I. Poberezhskiy, A. J. Riggs, N. Saini, E. Sidick,

- H. Tang, and J. Trauger, "WFIRST coronagraph flight performance modeling," *Proc. SPIE* **10698**, 106982K (2018).
20. J. H. Debes, M. Ygouf, E. Choquet, D. C. Hines, M. D. Perrin, D. A. Golimowski, C.-P. Lajoie, J. Mazoyer, L. Pueyo, R. Soummer, and R. van der Marel, "Wide-field infrared survey telescope-astrophysics focused telescope assets coronagraphic operations: lessons learned from the Hubble Space Telescope and the James Webb Space Telescope," *J. Astron. Telesc. Instrum. Syst.* **2**, 011010 (2015).
 21. Q. Gong, D. A. Content, M. Dominguez, T. Emmett, U. Griesmann, J. Hagopian, J. Kruk, C. Marx, B. Pasquale, T. Wallace, and A. Whipple, "Wide-field infrared survey telescope (WFIRST) slitless spectrometer: design, prototype, and results," *Proc. SPIE* **9904**, 990412 (2016).
 22. Physik Instrumente (PI), *H-811 Hexapod Microrobot: User Manual* (PI, 2013).
 23. Physik Instrumente (PI), *M-850 & M-840 Hexapod 6-Axis Positioning Systems: User Manual* (PI, 2003).